JOURNAL OF APPLIED ELECTROCHEMISTRY 25 (1995) 1045–1051

Voltammetric study of the Fe–S–Ebonex® system

A. GOMES, M. I. DA SILVA PEREIRA, M. H. MENDONÇA, F. M. A. COSTA

Departamento de Química, Faculdade de Ciências da Universidade de Lisboa, Rua Ernesto Vasconcelos, Ed. C1, 1700 Lisboa, Portugal

Received 25 October 1994; revised 7 March 1995

A voltammetric study of the Fe–S–Ebonex® system at pH 3 is reported. Aqueous solutions of $Na_2S_2O_3$ and $(NH_4)_2Fe(SO_4)_2$ were used as sources of sulphur and iron, respectively. The influence of the starting potential on the electrochemical behaviour of the system is analysed. Deposits obtained at −1.1 V vs SCE, by potentiostatic methods, show X-ray diffraction peaks of the pyrite structure. Troilite and mackinawite phases are also identified.

1. Introduction

The high costs of conventional solar cells make it necessary to investigate alternative production methods and materials with respect to their suitability for solar energy conversion.

In recent years there has been a considerable interest on the electrodeposition of thin film semiconductors of metallic chalcogenides. This technique has some advantages such as low cost and achievement of high purity semiconductor materials. Several composites have been synthesized by electrodeposition [1].

Iron sulphides, are semiconductors which show band gap values suitable for applications on solar energy conversion namely the FeS_2 (pyrite) [2]. Several attempts have been done to electrodeposit pyrite thin films, but with little success due in part to the formation of nonstoichiometric films and or contamination by other phases [3–6].

In this paper we report a preliminary study of the electrodeposition of iron sulphides on Ebonex® substrate from acidic aqueous solution. Ebonex® is a chemically inert conductive ceramic material based on the Magneli phases suboxides of titanium, of the general formula Ti_xO_{2x-1} [7]. Recent studies have shown that it presents interesting properties as an electrode material such as good adhesion in electrodeposition of metals [7, 8].

Moreover Ebonex® has a high overpotential for hydrogen evolution from aqueous solutions what makes it a suitable substrate for cathodic deposition [9]. On the other end pyrite formation has been observed at an interface involving an oxide of titanium in aqueous solution [10].

2. Experimental details

Electrochemical measurements were performed using a conventional three-electrode cell containing a commercial saturated calomel electrode (SCE) as a reference and a platinum mesh as counter electrode. The cell was connected to a low noise operational amplifier potentiostat programmed by a Wenking (model VSG 83) wave form generator and a Philips (model PM 8271) XY–t recorder. All potentials are reported with respect to the SCE.

The working electrode was an Ebonex® disc (Ebonex Technologies Inc.) of 6 mm diameter. The external contact to the Ebonex® disc was made either using an In/Ga eutectic baked with silver epoxy resin or a clean stainless steel rod, sharply pointed at one end, which rested on the reverse side of the disc. Before each experiment, the working electrode was polished with abrasive paper, washed with Millipore water, followed by ultrasonication.

Three aqueous solutions were studied: (i) 0.01 mol dm^{-3} $(NH_4)_2Fe(SO_4)_2$ and 0.01 mol dm^{-3} $(NH_4)_2SO_4$; (ii) 0.35 mol dm^{-3} $Na_2S_2O_3$ + 0.75 mol dm^{-3} Na_2SO_4 and (iii) 2.5×10^{-3} mol dm^{-3} $(NH_4)_2Fe(SO_4)_2$ + 0.26 mol dm^{-3} $Na_2S_2O_3$ + 0.56 mol dm^{-3} Na_2SO_4, with pH adjusted to about 3.0 with H_2SO_4. Solutions were prepared from AnalaR reagents with Millipore water and degassed with nitrogen.

All measurements were performed at room temperature.

The structural characterization of the electrodeposits films on Ebonex® support was done by X-ray powder diffraction using a Philips PW 1730 diffractometer with Cu$K\alpha$ radiation.

3. Results and discussion

3.1. *Voltammetric studies*

3.1.1. Electrode electrochemical characterization. To test the electrode response, the hexacyanoferrate redox system was employed as a model. Fig. 1 shows voltammograms obtained with an electrode with an In/Ga contact. The oxidation–reduction process gives rise to a pair of peaks superimposed on the background current due to the double-layer charging. A peak separation of 250 mV was determined for curve (a). This value accounts for the irreversibility of the system on the Ebonex®. Similar conclusions are referred in the literature [7, 8].

0021-891X

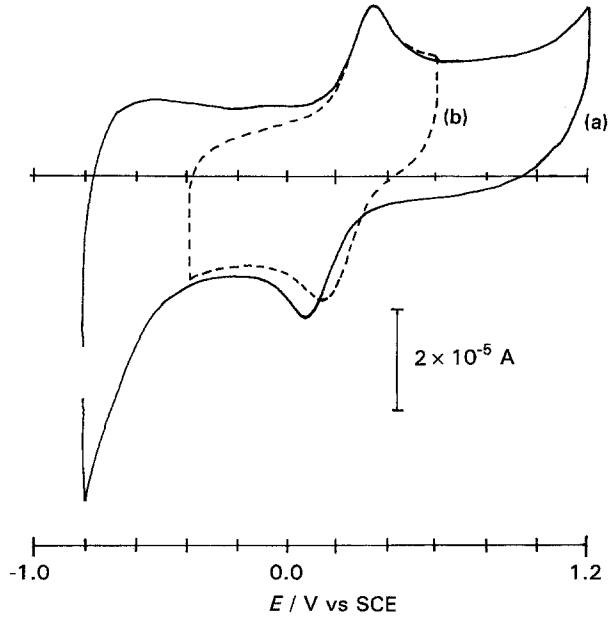

Fig. 1. Cyclic voltammograms for Ebonex® in 1×10^{-3} mol dm^{-3} $K_3[Fe(CN)_6] + 1$ mol dm^{-3} KCl, pH 3 showing the effect of the potential limits. Sweep rate 10 mV s^{-1}. Electrode geometric area: 0.28 cm^2.

Higher values for the peak separation were observed when the electrode external contact was made using a stainless steel rod. This behaviour led us to conclude that the contact resistance has a marked influence on the quality of results. Thus, all

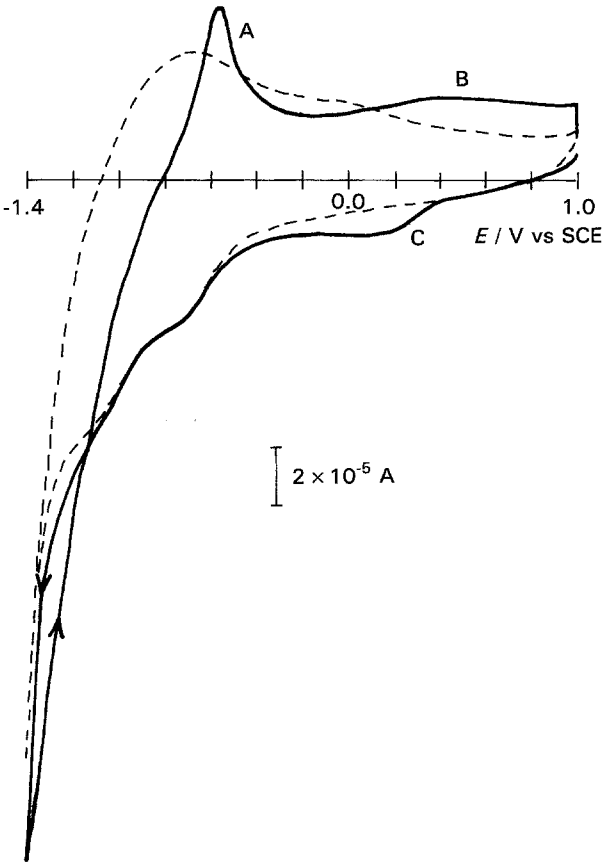

Fig. 2. Cyclic voltammograms for Ebonex® in 0.01 mol dm^{-3} $(NH_4)_2Fe(SO_4)_2$ (full line) and 0.01 mol dm^{-3} $(NH_4)_2SO_4$ (dashed line) at pH 3. Sweep rate 10 mV s^{-1}. Electrode geometric area: 0.28 cm^2.

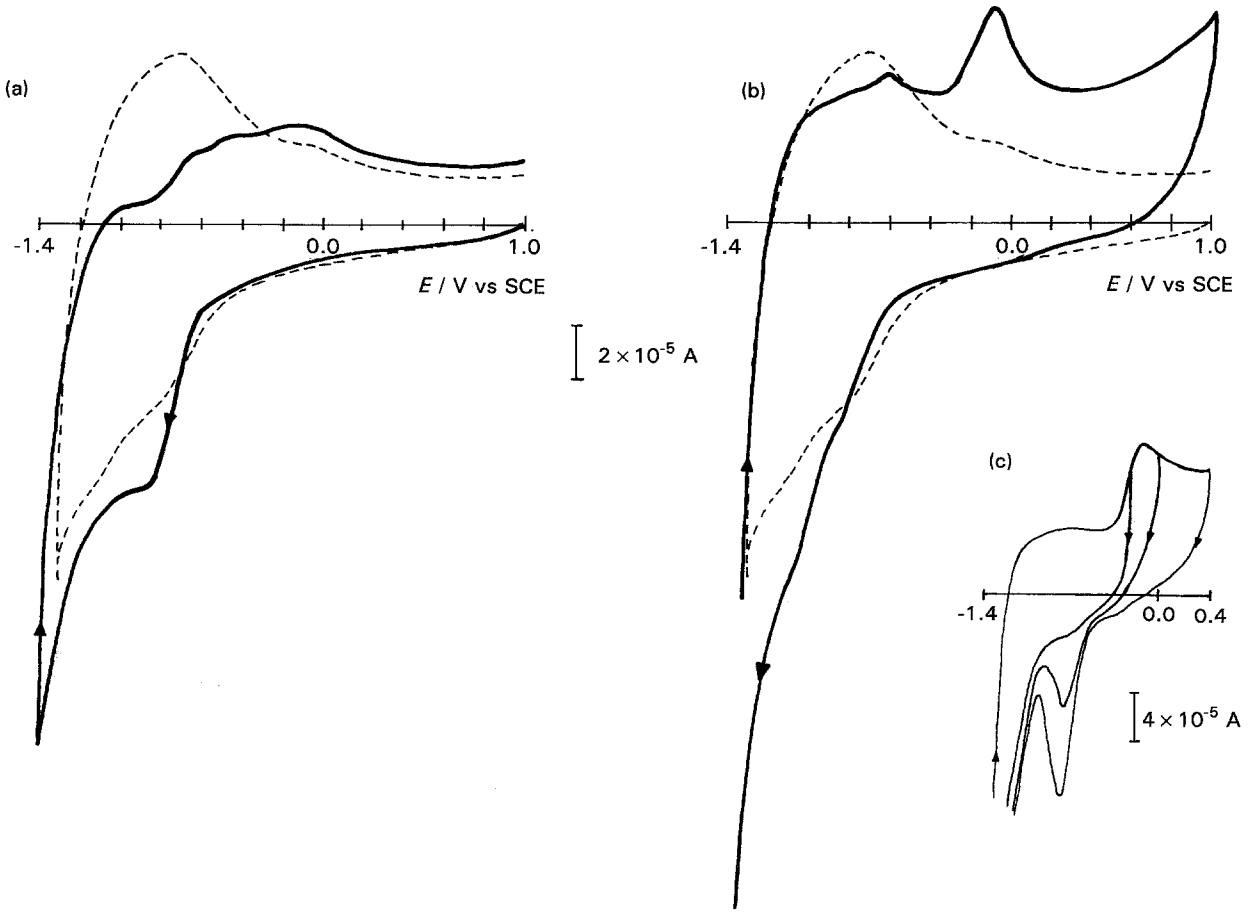

Fig. 3. Cyclic voltammograms for an Ebonex® electrode in 0.35 mol dm^{-3} $Na_2S_2O_3 + 0.75$ mol dm^{-3} Na_2SO_4 (pH 3), starting at (a) the positive limit, (b) the negative limit, dashed line corresponds to base electrolyte, and (c) showing the effect of the scan positive limit. Sweep rate: 10 mV s^{-1}. Electrode geometric area: 0.28 cm^2.

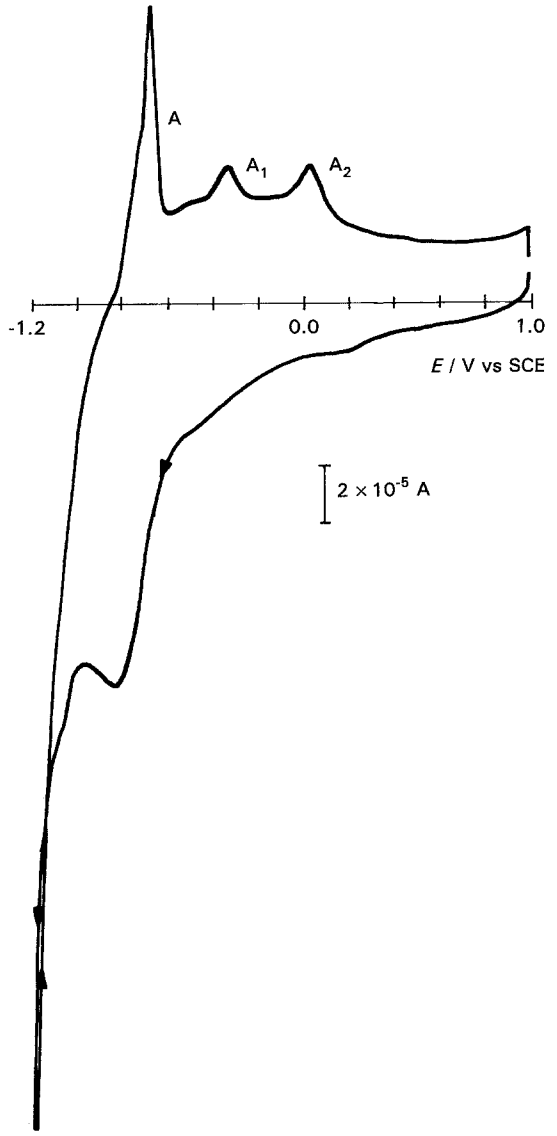

Fig. 4. Cyclic voltammogram for Ebonex® in 2.5×10^{-3} mol dm^{-3} $(NH_4)_2Fe(SO_4)_2$ + 0.26 mol dm^{-3} $Na_2S_2O_3$ + 0.56 mol dm^{-3} Na_2SO_4, pH 3. Sweep rate: 10 mV s^{-1}. Electrode geometric area: 0.28 cm^2.

the following measurements were performed with the In/Ga contact electrodes.

The influence of the potential scan limits on the electrochemical behaviour of the system was also investigated.

It was observed that the peak separation depends on the potential range and, more significantly, on the positive potential limit. Values of 160 mV, obtained from voltammograms run over a restricted potential interval (b), contrast with the value of 250 mV obtained during the sweep over an extended potential range as shown in Fig. 1.

This behaviour may be associated with the Ebonex® surface modification at high positive potentials due to a change in the Ti oxidation state, which affects the subsequent reactions of the system [7, 11]. Based on XRD studies Pletcher *et al.* [7] concluded that when Ebonex is anodised, the amount of Ti_4O_7 decreases substantially and higher titanium oxide forms predominate. Thus, the voltammograms, unless otherwise stated, were recorded after complete stabilisation of the electrode surface, that is, when the response was reproducible (3rd cycle).

3.1.2. Cyclic voltammetry of the iron/Ebonex® system. Figure 2 shows representative cyclic voltammograms for an Ebonex® electrode in aqueous solution containing 0.01 mol dm^{-3} $(NH_4)_2Fe(SO_4)_2$ (full line) and 0.01 mol dm^{-3} $(NH_4)_2SO_4$ (dashed line) at pH 3, starting with a cathodic sweep.

Comparison of the two curves clearly shows the presence of iron. A peak (C) and a shoulder followed by a loop, characteristic of a nucleation process, can be identified on the cathodic sweep. On the anodic scan, a well defined peak (A) and a broad one (B), are observed.

A detailed study, of the influence of the potential limits on the electrochemical behaviour of the system $(NH_4)_2Fe(SO_4)_2$/Ebonex® was made. This showed that the broad anodic peak (B) at about 0.40 V is

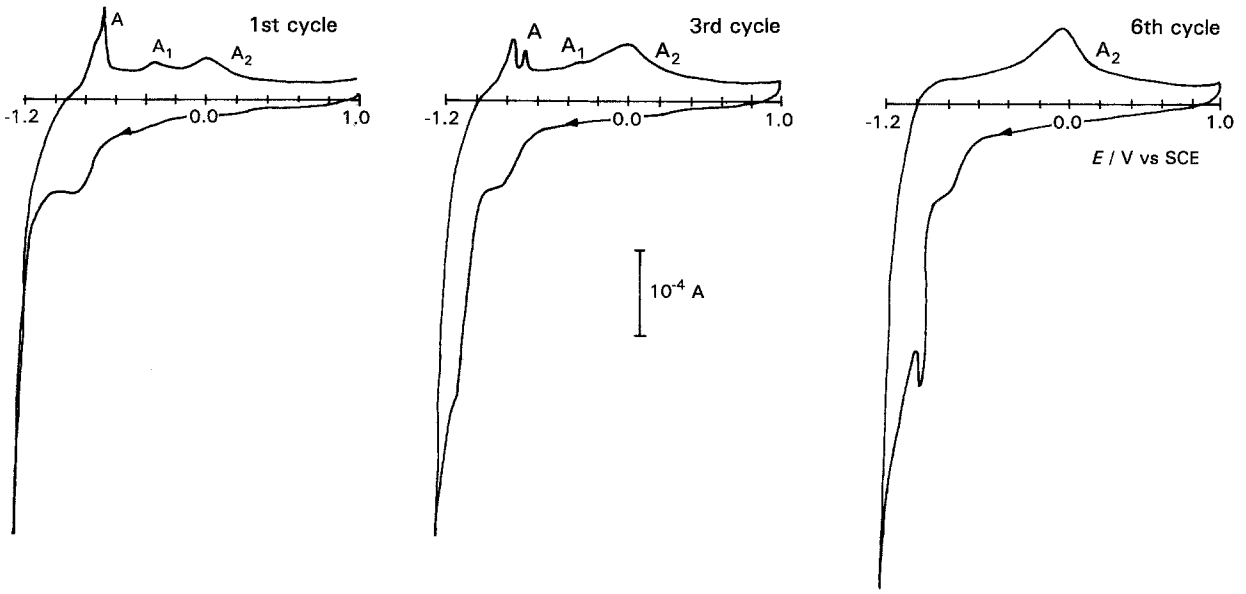

Fig. 5. Repetitive cyclic voltammograms for Ebonex® in 2.5×10^{-3} mol dm^{-3} $(NH_4)_2Fe(SO_4)_2$ + 0.26 mol dm^{-3} $Na_2S_2O_3$ + 0.56 mol dm^{-3} Na_2SO_4, pH 3. Sweep rate: 10 mV s^{-1}. Electrode geometric area: 0.28 cm^2.

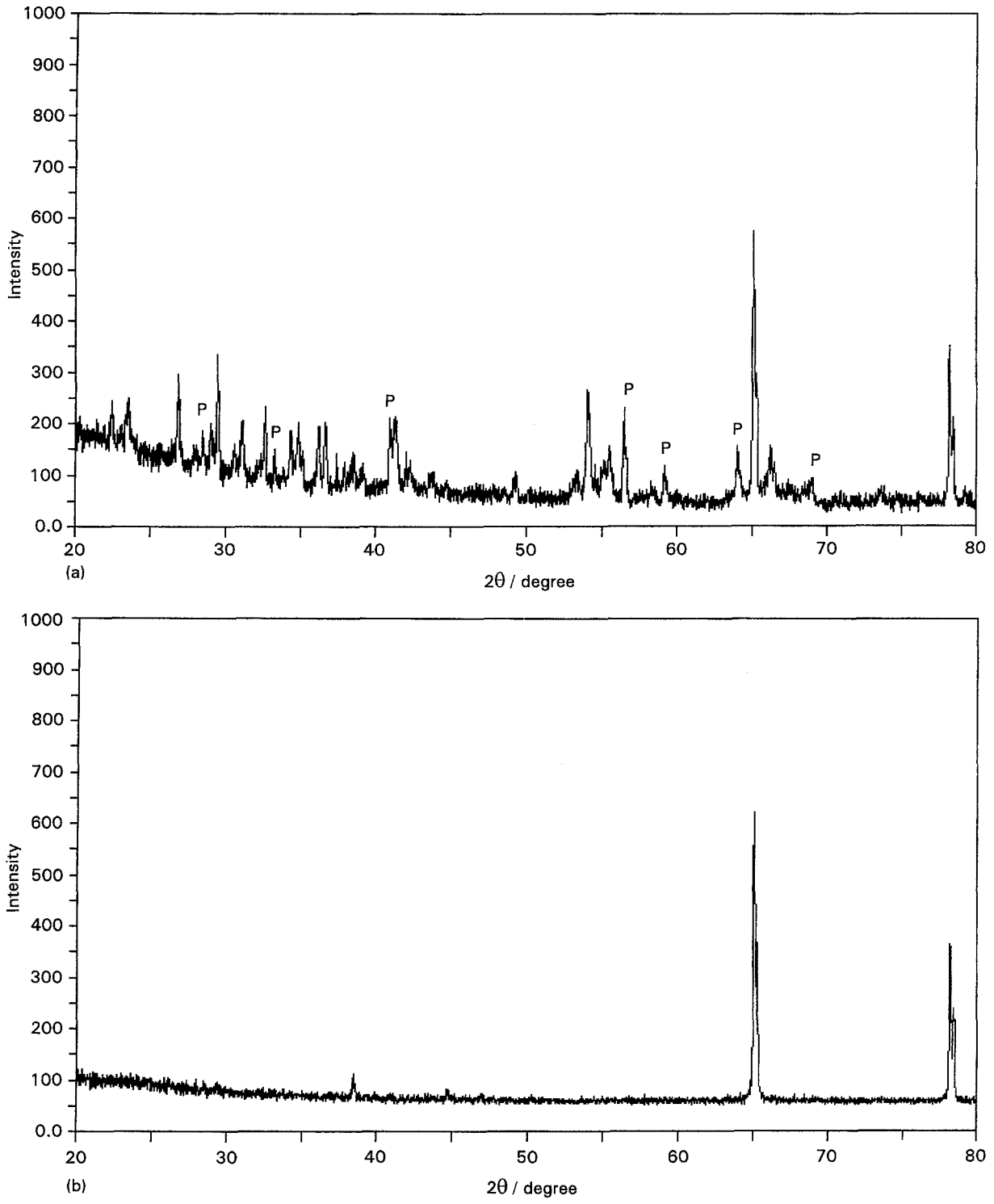

Fig. 6. XRD patterns of (a) electrodeposited film on the Ebonex® surface at −1.1 V vs SCE during 22 h, (b) samples holder and (c) clean Ebonex® surface.

Table 1. d spacing and h, k, l for FeS_2

hkl	d_{obs} /nm	d_{calc} /nm
111	0.3127	0.3127
200	0.2690	0.2708
211	0.2205	0.2211
311	0.1629	0.1633
222	0.1561	0.1563
321	0.1454	0.1447
420	0.1218	0.1211

associated to the cathodic peak (C) at about 0.20 V, and may be ascribed to the Fe(III)/Fe(II) couple.

Increasing the switching potential, a nucleation loop for iron deposition is observed and the respective anodic dissolution peak (A) appears at −0.60 V, on the return sweep.

At lower potentials, hydrogen evolution occurs simultaneously with iron deposition. This is confirmed by the formation of gas bubbles on the electrode surface. The shoulder observed on the cathodic run between −0.60 and −0.80 V, on both

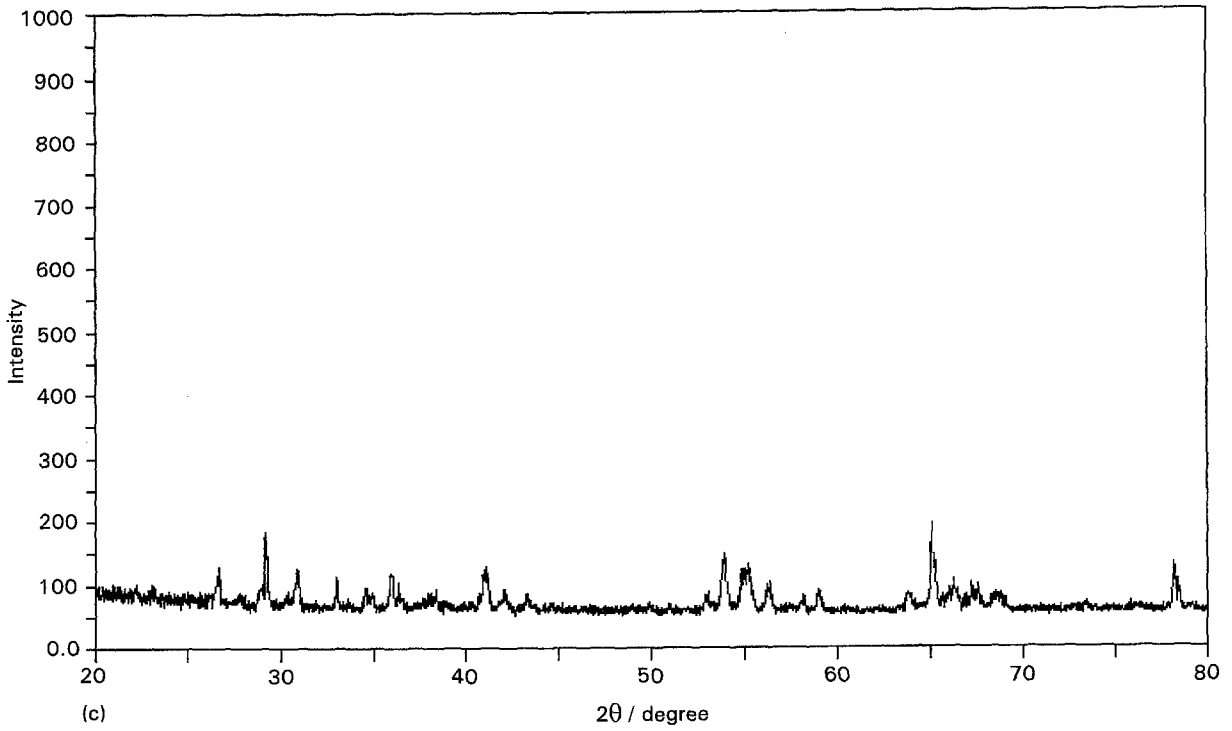

Fig. 6. Continued.

solutions, is clearly due to the reduction of the Ebonex® surface.

3.1.3. Cyclic voltammetry of the thiosulphate/Ebonex® system. The voltammetric behaviour of the 0.35 mol dm^{-3} $Na_2S_2O_3$ + 0.75 mol dm^{-3} Na_2SO_4/Ebonex® system was investigated taking into account that the thiosulphate ion is not stable in acidic media and decomposes into colloidal sulphur and HSO_3^- [12–14]:

$$S_2O_3^{2-}(aq) + H^+(aq) \rightleftharpoons S(\text{colloidal}) + HSO_3^-(aq)$$

Moreover, at pH 3 an equilibrium between HSO_3^- and H_2SO_3 also occurs [15].

Thus, the electrolyte solution is a complex mixture of species, $S_2O_3^{2-}$, HSO_3^-, H_2SO_3 and colloidal S. From the estimated standard potential stability range for the different species, adjusted to the solution pH, it is expected that H_2SO_3 is the first species to be reduced, followed by HSO_3^-, $S_2O_3^{2-}$ and, finally, the colloidal sulphur [16, 17].

Figure 3 shows voltammograms for an Ebonex® electrode in 0.35 mol dm^{-3} $Na_2S_2O_3$ + 0.75 mol dm^{-3} Na_2SO_4, starting at the positive limit (Fig. 3(a)) and at the negative limit (Fig. 3(b) and (c)). A voltammogram in the base electrolyte is also included (dashed line).

When the scan starts with a cathodic sweep it is clear that up to −0.40 V there is no difference in the currents obtained in the base electrolyte and in the thiosulphate solutions. At more negative potentials a bigger increase in current is observed for thiosulphate solutions and a defined peak appears at about −0.80 V, followed by an increase of current, much more pronounced than in the base electrolyte. This peak has been ascribed to the sulphur reduction, according to the following reaction [16–18]

$$S + 2H^+ + 2e^- \longrightarrow H_2S$$

At more negative potentials the reduction of sulphur to HS_x^- species ($1 \leqslant x \leqslant 5$) is also possible according to Henmingsen [16], and the following the reaction scheme

$$xS + H^+ + 2e^- \longrightarrow HS_x^-$$

The corresponding oxidation process is noticed on the anodic sweep between −0.80 V and −0.40 V. The shoulder observed at more positive values is, in part, also due to the surface oxidation, as can be seen when the curves are compared. On the other end, in the negative potential range, the current associated to the surface oxidation, decreases in the presence of the thiosulphate solution. This inhibition effect may be due to the sulphur at the electrode surface that is not completely reduced during the cathodic sweep.

The results obtained when the cyclic voltammogram is run starting at −1.30 V, and scanned in the positive direction, are presented in Fig. 3(b). In contrast with the results shown in Fig. 3(a), the anodic current is much higher, the anodic peaks better defined and the cathodic peak more drawn out. A much better definition is observed for the cathodic peak when the switching potential is less positive as Fig. 3(c) shows and a shift towards the negative potential is seen with increase in the film thickness. This may be due either to a change in the Ebonex® surface or to the nature of the film.

On Fig. 3(a) and (b) there is no evidence for electron transfer process evolving $S_2O_3^{2-}$, H_2SO_3 and HSO_3^-

species. This result suggests that the sulphur present on the Ebonex® surface may act as an inhibitor for these processes. Inhibition by sulphur has been observed on other substrates [3, 19–23].

3.1.4. Cyclic voltammetry of the iron + thiosulphate/Ebonex® system. Figure 4 shows a cyclic voltammogram for Ebonex® in 2.5×10^{-3} mol dm^{-3} $(NH_4)_2Fe(SO_4)_2$ + 0.26 mol dm^{-3} $Na_2S_2O_3$ + 0.56 mol dm^{-3} Na_2SO_4 at pH 3.

Starting from the positive potential and going in the negative direction, the peaks corresponding to the reduction of Fe(III) and sulphur, are clearly seen at about 0.19 V and −0.80 V, respectively, similar to those obtained when the solutions were not mixed (Figs 2 and 3(a)). However, the reduction of Fe(II) to Fe(0) is observed at a potential less negative than in the absence of thiosulphate. A similar effect was observed by Itabashi at the Hg electrode [24] and explained in terms of the formation of an iron sulphide film on the electrode surface that stimulates the reduction of Fe(II) to Fe(0).

The anodic region presents three well defined peaks A, A_1 and A_2. The peak assignment was done by comparison with the results obtained, for each single system. On this basis, peak A was attributed to the reoxidation of Fe(0) and peak A_2 to sulphur deposition. The shift towards more negative potentials observed for peak A, is analogous to that observed for the Fe(II)/Fe(0) couple in the cathodic scan, and probably due to a catalytic effect of the formed iron sulphide.

Since peak A_1 does not appear when each electrolyte was studied individually it was assigned to the iron sulphide oxidation according to

$$Fe_xS_y \longrightarrow xFe^{2+} + yS + 2xe^-$$

Sulphur would grow heterogeneously to provide porosity and access of solution to the electrode surface, for the subsequent sulphur deposition (A_2).

The effect of multicycling is shown in Fig. 5. Only the 1st, 3rd and 6th cycles are presented for clarity. As can be seen, the shape of the voltammogram changes with the scan number. Peak A deconvolutes into two peaks on the second cycle and disappears at above the fifth cycle. Peak A_1 changes to a broad wave and merges with peak A_2 and progressively increases.

The deconvolution of peak A may result from the difference in the reoxidation rates of Fe(0) at the Ebonex electrode covered with iron sulphide and the Ebonex® electrode. A similar result was obtained by Winkler *et al.*, for the Fe(II)–SCN^- system on a glassy carbon electrode. The presence of FeS on the glassy carbon surface leads to the appearance of two oxidation peaks for iron [25].

On the cathodic side, the most interesting feature is the development of the hump into a sharp peak just prior to iron reduction. This may be due to the reduction of sulphur deposited on the iron sulphide film.

After the 5th cycle a black precipitate was clearly seen on the vicinity of the electrode corresponding to the formation of iron sulphides by a dissolution-precipitation mechanism.

It is reasonable to suppose that after the 6th cycle the electrode surface is partially blocked by sulphur.

3.2. *Potentiostatic deposition and XRD characterisation of the film*

Potentiostatic studies were performed to identify the nature of the black film formed on the electrode surface. The deposition was performed in the potential range where iron ions coexist with sulphur reduced species. This is in accordance with the thermodynamic study of Kröger for the cathodic deposition of binary compounds [26].

Based on the voltammetric data, the deposition potential (E_{dep}) was placed in the potential range limited by −0.80 V and −1.10 V vs SCE. Before applying E_{dep} to the cell the electrode was multicycled between 0.00 V and −1.10 V, to condition its surface.

Structural characterisation, by X-ray powder diffraction, was carried out for several electrodeposits obtained under the same conditions as those described above, and similar diffractograms were always obtained.

A typical XRD pattern of the electrodeposit is presented on Fig. 6(a). Figure 6(b) and (c) are the X-ray powder diffractograms of the Ebonex® and sample holder respectively, before the electrodeposition procedure.

Excluding the peaks of the substrate and the holder from the diffractogram of the deposit (Fig. 6(a)) the remaining diffraction lines may be indexed as: (i) the cubic phase FeS_2, pyrite (P) according to the ASTM file 6-710, as shown on the Table 1, and (ii) some diffraction lines of troilite (FeS) and mackinawite ($Fe_{1+x}S$) according to the ASTM files 11-151 and 15-037, respectively.

The remaining lines, which do not correspond to any known sulphide, should correspond to the modified Ebonex® (TiO_x) surface, due to the oxidation of the mixed titanium oxides [7].

4. Conclusion

In this work a mixture of crystalline iron sulphides was obtained by electrodeposition in potentiostatic conditions from aqueous solutions containing sulphur and iron(II), as prevailing species. Pyrite, mackinawite and troilite were identified by XRD studies.

Cyclic voltammetric studies led to the conclusion that the iron sulphide formation occurs during the course of the electroreduction of the sulphur in the presence of metal ions.

Experiments are in progress towards a more complete characterization of the system in order to control the composition of the deposits and optimise the formation of pyrite.

Acknowledgement

This work was partially supported by JNICT under research project CIÊNCIA 100/C/92.

References

[1] C. D. Lokhande and S. H. Pawar, *Phys. Stat. Sol.* **111** (1989) 17.
[2] A. Ennaoui, S. Fiechter, Ch. Pettenkofer, N. Alonso-Vante, K. Buker, M. Bronold, Ch. Höpfner and H. Tributsh, *Sol. Energy Mater. Sol. Cells* **29** (1993) 289.
[3] A. S. Aricò, V. Antonucci, P. L. Antonucci, D. L. Cocke and N. Giordano, *Electrochim. Acta* **36** (1991) 581.
[4] S. N. Sahu and C. Sanchez, *J. Mater. Sci. Lett.* **11** (1992) 1540.
[5] N. R. de Tacconi, O. Medvedko and K. Rajeshwar, *J. Electroanal. Chem.* **379** (1994) 545.
[6] A. S. Aricò, V. Antonucci, P. L. Antonucci, E. Modica, S. Ferrara and N. Giordano, *Mat. Letters* **13** (1992) 12.
[7] J. E. Graves, D. Pletcher, R. L. Clarke and F. C. Walsh, *J. Appl. Electrochem.* **21** (1991) 848.
[8] R. René Miller-Folk, R. E. Noffle and D. Pletcher, *J. Electroanal. Chem.* **274** (1989) 257.
[9] R. J. Pollock, J. F. Houlihan, A. N. Bain and B. S. Coryea, *Mat. Res. Bull* **19** (1984) 17.
[10] A. G. Wikjord, T. E. Rummery and F. E. Doern, *Can. Mineralogist* **14** (1976) 571.
[11] J. Przyluski and K. Kolbrecka, *J. Appl. Electrochem.* **23** (1993) 1063.
[12] F. Johnston and L. McAmish, *J. Coll. Interf. Sc.* **42** (1973) 112.
[13] G. P. Power, D. R. Peggs and A. J. Parker, *Electrochim. Acta* **26** (1981) 681.
[14] E. Fatas, P. Herrasti, F. Arjona and E. G. Camarero, *J. Electrochem. Soc.* **134** (1987) 2799.
[15] T. Hemmingsen, *Electrochim. Acta* **37** (1992) 2785.
[16] *Idem, ibid.* **37** (1992) 2775.
[17] R. J. Biernat and R. G. Robins, *ibid.* **14** (1969) 809.
[18] M. Pourbaix, 'Atlas of electrochemical equilibria in aqueous solutions', Nace (1974).
[19] P. Marcus and E. Protopopoff, *Surf. Sci.* **161** (1985) 533.
[20] E. Lamy-Pitara, L. Bencharif and J. Barbier, *Electrochim. Acta* **30** (1985) 971.
[21] E. Lamy-Pitara and J. Barbier, *ibid.* **31** (1986) 717.
[22] I. C. Hamilton and R. Woods, *J. Appl. Electrochem.* **13** (1983) 783.
[23] M. Takahashi, Y. Ohshima, K. Nagata and S. Furuta, *J. Electroanal. Chem.* **359** (1993) 281.
[24] E. Itabashi, *ibid.* **103** (1979) 185.
[25] K. Winkler, S. Kalinowski and T. Krogulec, *ibid.* **252** (1988) 303.
[26] F. A. Kröger, *J. Electrochem. Soc.* **125** (1978) 2028.